

# CFA/VISHNO 2016

## Contrôle passif avec un NES fortement non linéaire

V. Iurasov, P.-O. Mattei et R. Côte

LMA Marseille, 4 impasse Nikola Tesla, 13453 Marseille, France  
iurasov@lma.cnrs-mrs.fr



LE MANS

The goal of this research is to apply the idea of energy pumping in vibroacoustics. Using a nonlinear dynamic absorber we want to control the low amplitude vibrations and the acoustic field emitted by a thin plate under acoustic excitation. We introduce a bi-stable nonlinear absorber. Its nonlinearity, that results in softening at low amplitudes of vibrations, allows to decrease considerably the threshold for the energy pumping. At higher level of excitation, we observe a chaotic regime in the absorber dynamics which leads to an unusual category of energy pumping. To illustrate the efficiency of the absorber we show the results of a recent experiment. To get access to the governing nonlinearity we develop a model of the bi-stable absorber. The obtained theoretical description of the absorber is in good agreement with our observations.

## 1 Introduction

Following the fundamental work of Gendelman *et al* [1, 2] on the energy pumping, the use of nonlinear systems as absorbers got a lot of interest from both scientific and industrial communities. The general name that was given to this type of absorbers is "Nonlinear Energy Sink" or simply "NES". The most simple NES involves a cubic nonlinearity that leads to an amplitude dependent resonance frequency. When the NES is coupled to a linear system, this dependence allows a resonance capture : at some amplitude of vibrations the NES resonance frequency becomes close to the one of the linear system and an energy transfer from the linear system to the NES occurs. The injected energy rises the amplitude of the NES vibrations and the corresponding frequency change breaks the resonance coupling. Thus the energy dissipates in the NES and can not be transferred back.

Beside this basic example, a variety of NESs with different types of nonlinearities was proposed, for example, NESs with quadratic and cubic nonlinearities in acoustic systems [3] or cubic NESs in mechanics [4].

The very recent numerical and theoretical work of Romeo *et al* [5] have shown that a bi-stable configuration, that possesses both quadratic and cubic nonlinearity, is able to solve the main limitation of the NESs - a high triggering threshold for energy pumping.

This paper presents the results of our work on a passive vibration control with a bistable NES developed by our group. We will start with the NES description and the presentation of the latest experimental results in the case of vibrations of an aluminum plate controlled by two NESs. In section 3 we propose a simple analytic model of a generalized linear system and of its coupling to the NESs. The linear vibration modes calculated for the NES (vibrations around the equilibrium position) are used to create a complete Galerkin discretization numerical model of the NES. Both the linear characteristics of the NES and the nonlinear ones are measured during a set of experiments presented in section 4. In the last section we briefly summarize the results.

## 2 Experimental setup

The NES we are working on is represented by the well-known bi-stable system - a buckled beam with fixed edges. The main modification that we introduce is to fix a significant mass on the buckled beam. Since the added mass is considerably bigger than the total mass of the beam, its dynamics is changed drastically when comparing with a case of a uniform beam. The detailed NES configuration is described in Figure.1. The initial configuration of the

bistable NES composed of a light steel blade with a mass placed at the center : length of the beam  $l = 10$  cm, thickness 0.13 mm, height 5 mm, midspan deflection  $\hat{b} = 2.35$  mm, the additional mass weights  $m_0 = 2.6$  g. The mass of the support that is clamping the beam edges is  $m_s = 30$  g.

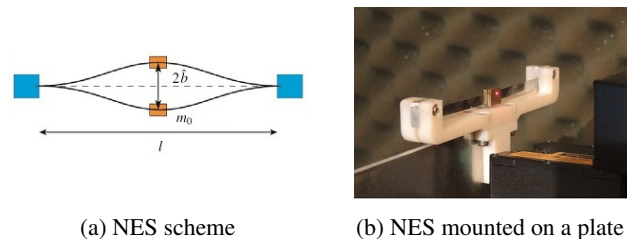


FIGURE 1 – The initial configuration of the bistable NES.

The experimental setup used to probe the NES efficiency is shown in Figure 2. An aluminum plate clamped from below and free from the other three sides was used as a linear system. The plate parameters were : thickness of 0.3 cm, width of 42 cm, height of 54.7 cm, total mass of 2070 g. A loudspeaker excited the plate vibrations. Two NESs were attached to the upper edges of the plate. The whole setup was mounted in an acoustically treated room. To avoid measuring the acoustic field reflected by the plate, the reference pressure was measured behind the loudspeaker close to its membrane. Two displacement laser sensors measured the displacements of the NESs centers, a velocimeter and an another displacement sensor traced the dynamics of one of the upper edges, a microphone measured the reference sound pressure created by the loudspeaker.



FIGURE 2 – The experimental installation.

The observed plate's linear vibration modes were in good correspondence with the ones predicted theoretically. The system behavior was explored around plate resonances of 43 Hz and 73 Hz which correspond to the plate's third and

fourth modes respectively. These modes have maximums at the NES attachment positions (see Figure 3).

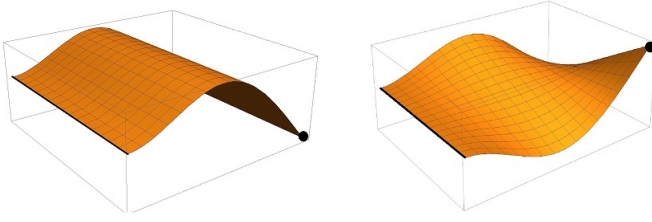


FIGURE 3 – The shapes of the third (left) and the fourth (right) modes of the plate. The solid black line identifies the clamped edge. The black dots indicate one of the NES attachment positions.

The loudspeaker provided a monochromatic excitation with a constant amplitude. Changing step by step the frequency and the amplitude we excited the system from the rest position and recorded first 21 seconds of signals. Eliminating the transients, we used the RMS of the plate's velocity to characterize its forced vibrations. In order to have the independent compartment of the NESs we performed measurements in different configurations via blocking and unblocking the NESs. The vibration response of the plate was characterized by a "response over signal" function  $RoS = 20 \log(V_{RMS}/SPL_{RMS})$ , where  $V_{RMS}$  and  $SPL_{RMS}$  are, respectively, the root mean square of the plate velocity and the root mean square of the excitation sound pressure level recorded during 10 seconds of forced plate vibrations. Figure 4 shows the ridge surface of this function in case of excitation around the fourth mode of the plate.

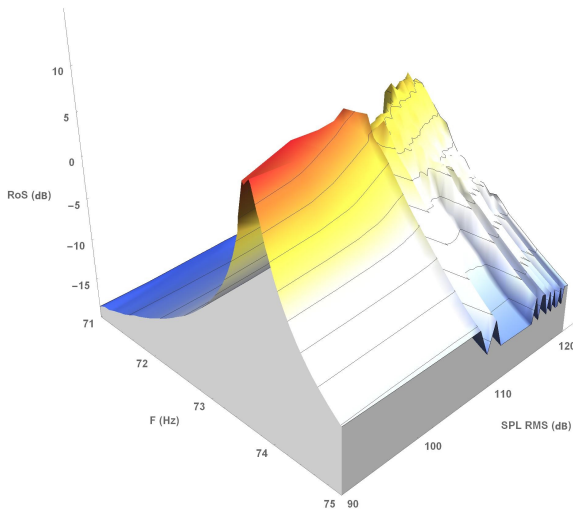


FIGURE 4 – Ridge surface for the plate response with both NESs unblocked as a function of the excitation frequency and the  $SPL_{RMS}$ .

Figure 5 illustrates the ridge curves for a case of one and two active NESs. We see that at high excitation levels we have an attenuation effect of up to 7 dB. This region corresponds to a regime in which NESs' motion becomes chaotic (see [7]). We also notice that the attenuation effect of NESs is cumulative.

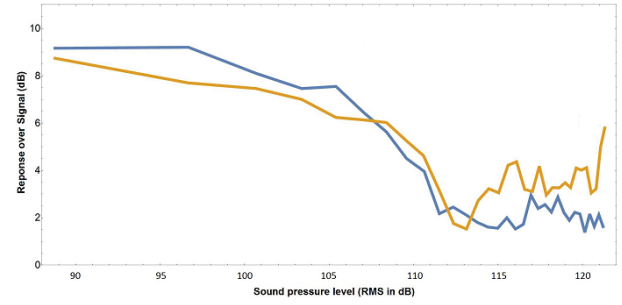


FIGURE 5 – The ridge curves for the fourth mode ridge surfaces. Curves : blue - both NESs are active, yellow - only one NES is active.

For the third mode the results are similar to the ones for the fourth mode. The sound pressure level threshold stays the same being around 105 – 110 dB, but the observed attenuation was considerably lower, staying around 2 dB. The lower attenuation is explained by the fact that, contrary to the fourth mode, the third mode is strongly coupled with the fluid. This way the NES damping effect will be relatively smaller when compared with the internal damping of the plate's vibration mode.

We should point out that, even though, the two NESs had very similar geometry, their observed linear vibration frequencies differed a lot being from 25 Hz up to 40 Hz, depending on the NES and its equilibrium position. This sensitivity of the NES properties to small changes of its geometry indicates that the one mode approximation, analyzed in [5], would give only a good qualitative illustration for the interaction between the plate and the NES, but it is not able to describe NES fine dynamics, such as the linear resonance frequencies or the triggering level. In the next section we propose a more refined model that can explain the apparent sensitivity and gives a quantitative description of the NES.

## 3 Modeling

### 3.1 General analytic description

It is easy to see that the difficulty for modeling the system "NES+plate" lays in the NES itself, while the linear system and its coupling are straightforward. Proceeding with a mode projection for the linear system in case of one NES we would formally obtain the following Lagrangian :

$$L = \sum_{i=1}^{N_i} \frac{M_i}{2} \left( \frac{\partial y_i(\hat{t})}{\partial \hat{t}} \right)^2 - \sum_{i=1}^{N_i} \frac{k_i y_i^2(\hat{t})}{2} + \frac{1}{2} \int_0^l m(\hat{x}) \left( \sum_{i=1}^{N_i} \frac{\partial y_i(\hat{t})}{\partial \hat{t}} + \frac{\partial \Phi(\hat{x}, \hat{t})}{\partial \hat{t}} \right)^2 d\hat{x} - U(\Phi(\hat{x}, \hat{t})). \quad (1)$$

Here  $y_i$ ,  $M_i$ ,  $k_i$  are the coordinate, mass and stiffness of the linear system mode number  $i$ . The projection was done such that  $y_i$  correspond to the mode displacements at the attachment point of the NES support.  $\Phi(\hat{x}, \hat{t})$  represents the transverse beam displacement as a function of coordinate along the beam  $\hat{x}$  and time  $\hat{t}$ .

To get the part of Lagrangian that describes the NES we suppose that the mass is point-like and the beam is

uniform : this allows us to use the equation for a clamped-clamped buckled beam as a base of our model. We also suppose that the boundary conditions are ideal. Under these approximations we can write the equation for a transverse planar vibrations of our NES [7] :

$$(m + \hat{M}\delta(\hat{x}-\hat{x}_0))\frac{\partial^2 \hat{w}}{\partial \hat{t}^2} + EI\frac{\partial^4 \hat{w}}{\partial \hat{x}^4} + P\frac{\partial^2 \hat{w}}{\partial \hat{x}^2} + \hat{c}\frac{\partial \hat{w}}{\partial \hat{t}} \quad (2)$$

$$= \frac{EA}{2l}\frac{\partial^2 \hat{w}}{\partial \hat{x}^2} \int_0^l \left(\frac{\partial \hat{w}}{\partial \hat{x}}\right)^2 d\hat{x} + \hat{F}(\hat{x}, \hat{t}),$$

with the boundary conditions

$$\hat{w} = 0 \text{ and } \frac{\partial \hat{w}}{\partial \hat{x}} = 0 \text{ at } \hat{x} = 0 \text{ and } \hat{x} = l. \quad (3)$$

Here  $m$  is the mass per unit length,  $\hat{w}(\hat{x}, \hat{t})$  is the transverse displacement at position  $\hat{x}$  at time  $\hat{t}$ ,  $E$  is the Young's modulus,  $A$  and  $I$  are the area and the moment of inertia of the cross section, respectively,  $l$  is the length of the non-deformed beam,  $\hat{P}$  is the axial load,  $\hat{c}$  is the viscous damping coefficient,  $\hat{F}(\hat{x}, \hat{t})$  is the external force.  $\hat{M}$  is the added mass and  $\hat{x}_0$  is the point of its attachment. Beside the presence of the  $\delta$ -part, it is the equation for a buckled clamped-clamped ideal beam (see [6]).

To simplify the expressions we will follow [6] using non-dimensional variables :

$$x = \frac{\hat{x}}{l}, \quad x_0 = \frac{\hat{x}_0}{l}, \quad w = \frac{\hat{w}}{r}, \quad t = \hat{t} \sqrt{\frac{EI}{ml^4}}, \quad (4)$$

$$\Omega = \hat{\Omega} \sqrt{\frac{ml^4}{EI}}, \quad M = \frac{\hat{M}}{ml},$$

where  $r = \sqrt{I/A}$  is the gyration radius of the beam cross section. Thus the Eqs.(2) and (3) will take form of a system

$$(1 + M\delta(x - x_0))\ddot{w} + w^{iv} + Pw'' \quad (5)$$

$$- \frac{1}{2}w'' \int_0^1 w'^2 dx = -c\dot{w} + F(x, t),$$

with  $w = 0$  and  $w' = 0$  at  $x = 0$  and  $x = 1$  and new non-dimensional quantities

$$P = \frac{\hat{P}l^2}{EI}, \quad c = \frac{\hat{c}l^2}{\sqrt{mEI}}, \quad F = \frac{\hat{F}l^4}{rEI}.$$

Here the dot indicates the derivative with respect to time, while the prime indicates a derivative with respect to coordinate  $x$ .

Now it is easy to define the shape of the static deformation, since in our approximation there is no effect of presence of the added mass. Dropping the dynamical terms we get well known equation for a uniform buckled beam :

$$w^{iv} + Pw'' - \frac{1}{2}w'' \int_0^1 w'^2 dx = 0. \quad (6)$$

The solutions of this problem are

$$w_{s_1}(x) = 0, \quad (7)$$

$$w_{s_2}(x) = \frac{b}{2}(1 - \cos 2\pi nx), \quad \text{where } (n \in \{1, 2, 3, 4, \dots\}), \quad (8)$$

$$w_{s_3}(x) = a \left( \sin kx - \frac{k}{2} \cos kx - kx + \frac{k}{2} \right), \quad (9)$$

where  $\tan k/2 = k/2$ .

Here  $w_{s_1}(x)$  is a trivial solution, while  $w_{s_2}(x)$  and  $w_{s_3}(x)$  are correspondingly the symmetric and the antisymmetric buckled configurations. The equilibrium positions are defined by the symmetric solution with  $n = 1$ , while the first antisymmetric solution will define the saddle points that "separate" them.

The equilibrium buckling gives us a useful relation between the unknown load and the measurable midspan deflection  $\hat{b} = rb$  :

$$\hat{P} = \frac{E\pi^2}{4l^2} (16I + A\hat{b}^2). \quad (10)$$

In order to find the linear vibration modes around the equilibrium position we will look for the solution in the form

$$w(x, t) = \frac{b}{2}(1 - \cos 2\pi x) + v(x, t). \quad (11)$$

Thus, the function  $v(x, t)$  that is searched in a form  $v(x, t) = \phi(x)e^{i\omega t}$  have to satisfy a linearized, undamped, unforced form of the Eq. (5) :

$$(1 + M\delta(x - x_0))\ddot{v} + v^{iv} + 4\pi^2 v'' \quad (12)$$

$$- 2b^2\pi^3 \cos 2\pi x \int_0^1 v' \sin 2\pi x dx = 0,$$

with  $\phi = 0$  and  $\phi' = 0$  at  $x = 0$  and  $x = 1$ .

The general solution of this equation at the limit  $M = 0$  is already known (see [6]) :

$$\phi_0(x) = \alpha \sin \lambda_1 x + \beta \cos \lambda_1 x \quad (13)$$

$$+ \gamma \sinh \lambda_2 x + \eta \cosh \lambda_2 x + \zeta \cos 2\pi x.$$

where

$$\lambda_1 = \sqrt{2\pi^2 + \sqrt{\omega^2 + 4\pi^4}}, \quad \lambda_2 = \sqrt{-2\pi^2 + \sqrt{\omega^2 + 4\pi^4}}.$$

It is easy to check that when  $M \neq 0$  the general solution takes form of

$$\phi(x) = \phi_0(x) + \frac{\omega^2 M}{4\sqrt{\omega^2 + 4\pi^4}} \phi_0(x_0) \Delta(x, x_0), \quad (14)$$

$$\text{with } \Delta(x, x_0) = \left( -\frac{1}{\lambda_1} \sin \lambda_1 |x - x_0| + \frac{1}{\lambda_2} \sinh \lambda_2 |x - x_0| \right).$$

Choosing  $\alpha_i$  as a free parameter (that corresponds to the amplitude of vibrations) and using the five equations provided by (12) we derive the coefficients  $\beta_i, \gamma_i, \eta_i, \zeta_i$  and the corresponding frequencies  $\omega_i$  for every mode number  $i$ . We define the scalar product in the solutions space as

$$(f, g) = \int_0^1 f(x)(1 + M\delta(x - x_0))g(x)dx, \quad (15)$$

so that after a normalization of our solutions we will obtain an orthogonality condition

$$(\phi_\alpha, \phi_\beta) = \int_0^1 \phi_\alpha(x)(1 + M\delta(x - x_0))\phi_\beta(x)dx = \delta_{\alpha\beta}. \quad (16)$$

It is worth noting from that the obtained modes are extremely sensitive to the mass position, particularly when the mass is placed close to the beam center (see Figure 6). This explains why we observed such a big difference in linear frequency for different NESs when the mass was fixed close to the beam center.

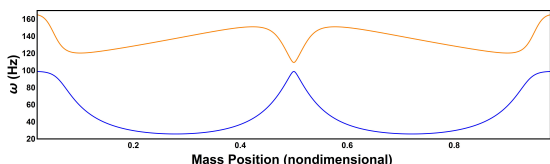


FIGURE 6 – The calculated resonance frequencies as a function of the non dimensional mass position. Curves : blue - first mode, orange - second mode.

### 3.2 Numerical model

To describe high amplitude vibrations of the NES we proceed with a discretization approach that uses the linear mode shapes as a base for the Galerkin method. The question of how many modes should be retained is quite subtle. The main requirements that we pose for the model is that it should describe both stable equilibrium positions. Since the unstable equilibrium positions (9) can be seen as characteristic for the snap-through motion, we should have them in the model as well. Finally, the equilibrium positions of the model should give us the linear vibration frequencies close to the ones calculated earlier. The final number depends a lot on the configuration, particularly on the value of the added mass, its position and the buckling level. This method applied for uniform beams with low buckling levels shows that 3 modes is already enough to meet the goals. In our case of high buckling and big added mass we need at least 50 modes, having less than 10% error on the frequency of the first mode.

In general case we write the solution of the problem as

$$w(x, t) = w_{s_3}^1 + \sum_{i=0}^N \phi_i(x) q_i(t), \quad (17)$$

where  $\phi_i(x)$  is the normalised spatial shape of the linear mode  $i$ ,  $q_i(t)$  is the corresponding time-dependent unknown variable,  $N$  is the number of retained modes and, finally,  $w_{s_3}^1$  is one of two unstable equilibrium positions that are the saddle points for the NES potential energy. Substituting expression 17 into the Eq. 5, multiplying by the normalized linear mode  $\phi_k$ , integrating over the space domain, using integration by parts and finally simplifying we get a system of  $N$  equations (the Einstein summation convention is used) :

$$\begin{aligned} \ddot{q}_k + \left( Z_{ki} - \left( P - \frac{1}{2} W_A \right) S_{ki} \right) q_i \\ + \frac{1}{2} (R_k + S_{ki} q_i) (2R_m q_m + q_n S_{nm} q_m) = \\ - c \Phi_{ki} \dot{q}_i + F_k(t), \end{aligned} \quad (18)$$

with

$$\begin{aligned} Z_{ki} &= \int_0^1 \phi_k''(x) \phi_i''(x) dx, & W_A &= \int_0^1 w_{s_3}^{1,2} dx, \\ S_{ki} &= \int_0^1 \phi_k'(x) \phi_i'(x) dx, & R_k &= \int_0^1 \phi_k'(x) w_{s_3}^{1'} dx, \\ \Phi_{ki} &= \int_0^1 \phi_k(x) \phi_i(x) dx, & F_k(t) &= \int_0^1 \phi_k(x) F(x, t) dx. \end{aligned} \quad (19)$$

Performing an orthogonal transformation on the  $q$  coordinates we can diagonalize  $S_{ki}$  that considerably simplifies further simulations.

## 4 The experimental tests of the model

To estimate the precision of our model we can start with a comparison of the obtained linear frequencies with the ones we observe experimentally at small vibration amplitudes. For this purpose we used a test NES configuration with a mass shifted from the center ( $x_0 = 0.35$ ). The comparison of the measured vibration responses and the predicted frequencies is given on Figure 7 ; Figure 8 shows the calculated spatial shapes of the modes for this test case.

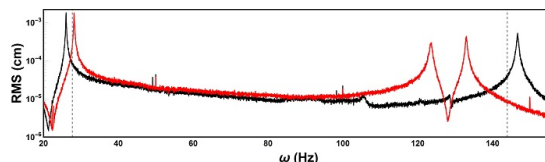


FIGURE 7 – The FFT for the NES displacement measured at the point  $x = 0.7$ . Curves : red - the first equilibrium position, black - the second ; dashed gray - calculated frequencies.

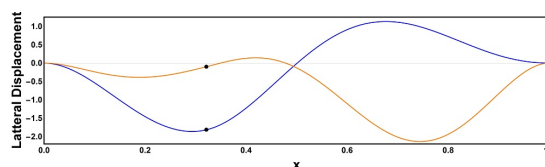


FIGURE 8 – Mode spatial shapes for the first (blue) and the second (orange) modes of the test NES. The black dot shows the position of the attached mass.

We can see that the model can describe the experimental results only to a certain extent, being limited by our approximation. We see that the asymmetry of the border conditions has an observable effect on the linear frequencies. It is worth to mention that the used beam is not completely uniform and has variations in its width of about 0.02 mm that gives a 10 – 15% error on the frequency. The peak at 105 Hz for the first equilibrium position cannot be predicted by our model since it corresponds to the torsion mode resonance of the beam, which is not taken into account in our model.

In order to test the numeric model we couple our test NES to a vibrating support, thus reducing the feedback of the NES and simplifying the analysis of the results. We perform a test with monochromatic excitation of constant amplitude around the first linear resonance of the NES (similar to the one done for the complete system). Figures 9 and 10 allows a qualitative comparison between the experimental and calculated responses of the NES. It is worth noting that we observe the same NES behavior without any optimization. This confirms the model's ability to describe NES dynamics at high excitation levels.

## 5 Conclusion

The experimental results show explicitly that the presented low mass bi-stable NES is able to considerably attenuate vibrations of a acoustically excited plate of much bigger dimensions. Planning to attack the modeling of the energy transfer we concentrate here on the NES properties and propose a model that is able to describe both, the linear

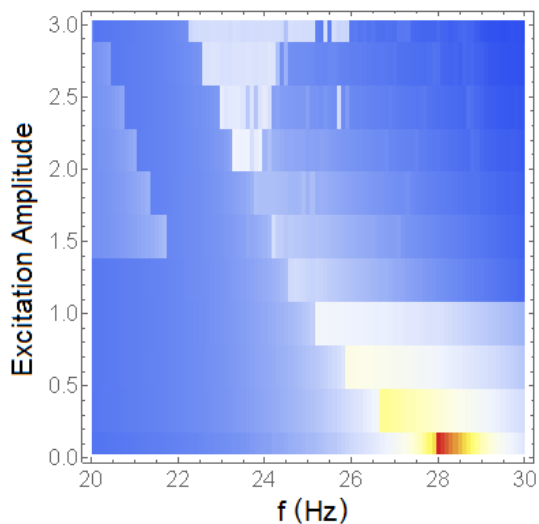


FIGURE 9 – The complete experimental dynamic density map as a function of frequency and amplitude of excitation.

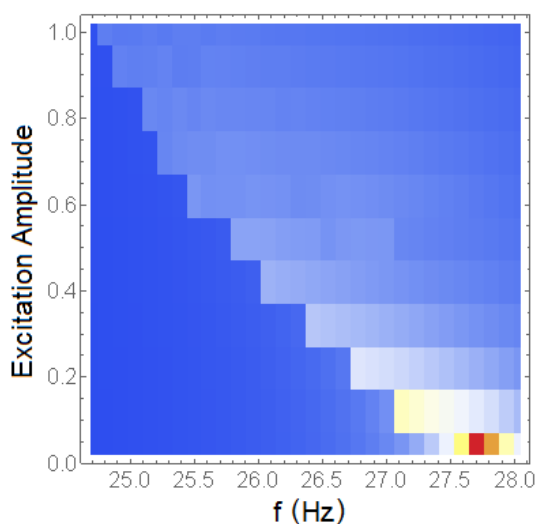


FIGURE 10 – The theoretical low amplitude dynamic density map as a function of frequency and amplitude of excitation.

and the nonlinear regimes. We validate the model by a set of experiments both in the linear and the nonlinear regimes.

## Références

- [1] O.V. Gendelman, L.I. Manevitch, A.F. Vakakis, R.M. Closkey, Energy pumping in nonlinear mechanical oscillators : Part I - Dynamics of the underlying Hamiltonian systems, *ASME Journal of Applied Mechanics* **68**, 34-42 (2001).
- [2] A.F. Vakakis, O.V. Gendelman, Energy pumping in nonlinear mechanical oscillators : Part II - Resonance capture, *ASME Journal of Applied Mechanics* **68**, 42-48 (2001).
- [3] P.-O. Mattei, R. Bellet, B. Cochelin, R.Côte, Enhancing targeted energy transfer by using several nonlinear membrane absorbers, *Proceedings of the Acoustics 2012 Nantes Conference*, <hal-00810706>, (2012).
- [4] A.F. Vakakis, O.V. Gendelman, L.A. Bergman, D.M. McFarland, G. Kerschen, Y.S. Lee, Nonlinear targeted energy transfer in mechanical and structural systems (two volumes), *Springer Verlag*, Berlin, (2004).
- [5] F. Romeo, L.I. Manevitch, L.A. Bergman and A. Vakakis, Transient and chaos low-energy transfers in a system with bistable nonlinearity, *Chaos* **25**, 053109 (2015).
- [6] S. A. Emam, A.H.Nayfeh, On the nonlinear dynamics of a buckled beam subjected to a primary-resonance excitation, *Nonlinear Dynamics* **35**, 1-17 (2004).
- [7] P.-O. Mattei, R.Ponçot, M.Pachebat, R. Côte, Nonlinear targeted energy transfer of two coupled cantilever beams coupled to a bistable light attachment, accepted for publication in *Journal of Sound and Vibration*, (2016).